Synthesis of CuO - Reduced Graphene Oxide Nanocomposite for High Performance Electrochemical Capacitors

M. Iniya Pratheepa[1], M. Lawrence[1]*

[1]*Department of Physics, St. Joseph's College (Autonomous), Tiruchirappalli, Tamilnadu*
E-mail: jefflara1968@yahoo.co.in

Abstract

A modified Hummers method has been proposed for preparing reduced graphene oxide (rGO) and the co-precipitation for Copper oxide (CuO) nanocomposites. The morphology of obtained nanocomposites was characterized by scanning electron microscope (SEM). X-ray powder diffraction (XRD) reveals the structural property. Fourier transform infrared spectrometer (FT-IR) used to investigate the functional groups of the materials. The optical property was confirmed by Ultra violet visible spectrum (UV). The optical band gap was observed to be 2.1 eV which was evaluated from Tauc's plot. It has been found that the morphology of the obtained structures can be modified by adjusting the synthesis conditions including the molar ratio of the starting materials. The charge storage ability, cycle stability and ion transport of the obtained rGO/CuO nanocomposites were investigated by methods of cyclic voltammetry (CV), galvanostatic charge-discharge curve and electrochemical impedance spectroscopy (EIS). It has been demonstrated that the charge storage ability of the product is firmly influenced by its morphology while the cycle stability is affected by crystallinity. The highest specific capacitance of nanocomposites was found to be 381.69 F/g at the nanoparticles scan rate of 10 mV/s.

Keywords: Modified Hummers method, rGO/CuO, XRD, Electrochemicalproperty, Electrochemical Capacitor.

*Corresponding Author
M. Lawrence
Department of Physics
St. Joseph's College (Autonomous)
Trichy- 620 002, Tamilnadu
E-mail : jefflara1968@mail.sjctni.edu
Contact Number : +91- 9842459119

1. Introduction

In the course of recent years, electrochemical capacitors are attracting wide attention, due to their high power density, excellent reversibility, and long cycle life, in order to solve environmental issues and the consumption of petroleum products [1]. As a rule, the energy density in view of pseudo- Faradic processes is usually many times greater than that of double-layer capacitors. To this end, much consideration is presently focused on the oxides of manganese, nickel, cobalt, vanadium, and copper [2-6] as a possiblity for the electrode materials of supercapacitors. At present, control over the shapes and structures of transition metal oxides has attracted significant interest in materials syntheses since the shape and size are imperative factors in determining the structural, physical, and chemical properties of nanomaterials [7]. The drawbacks affecting the application of transition metal oxides for supercapacitors are their poor electronic conductivities and large volume variation during the charge-discharge process, which leads to severe mechanical strains and very rapid capacitor decay.8 Experimentally, general modification techniques involve the synthesis of nanostructured materials, raising the specific surface area (SSA), and the addition of carbonaceous materials with high electrical conductivity and elastic buffers [9–11]. However, nanoparticles might be pulverized severely during cycling, which will negate the benefits of the decreased particle size. Furthermore, the large SSA of these progressive nanostructures has so far ended up being extremely effective in upgrading the cycle capacity of transition metal oxide based electrodes for energy storage devices [10,11].

As an imperative p-type transition-metal oxide with a narrow band gap ($Eg¼1.2$ eV), CuO has been generally utilized as a part of active anode materials, superconductors, sensors and heterogeneous catalysts. It is likewise a promising material for fabricating solar cells, because of its photoconductive and photochemical properties [12–16]. Specifically, CuO has been investigated as an electrode material for high-power electrochemical pseudocapacitors because of its inexhaustible assets, environmental compatibility, cost adequacy and ideal pseudocapacitive characteristics [17–19]. Like other metal oxides, it is important for CuO based pseudocapacitors to accomplish high specific surface area, high electrical conductivity, and a fast cation diffusion process to achieve high power densities and energy densities. Current research work has been for the most part focused on improving the electronic conduction of the electrodes using metal [20] and CNT doping [19,21].

Currently, graphene nanosheets (GNS) primarily based on transition metal oxides [22,23] have been studied and are anticipated to expose progressed capacitance owing their improved electronic conductivity, due to graphene

materials owning rapid electron transfer, high mechanical strength, high elasticity, and large surface area. Integrating graphene into functional architectures and composites currently has been a lively research area [24-26].

In this work, we document a facile co precipitation technique for the synthesis of hexagonal nanostructure copper oxide– reduced graphene to be used in supercapacitors. The "oriented attachment" mechanism is liable for the architecture formation. The nanocomposites with a new 2d nanostructure solve the problem of aggregation, and high specific capacitance may be expected due to the high electrical conductivity of the graphene matrix. The acquired CuO/rGO nanocomposites may have potential packages in catalysts, sensors, and lithium ion electrode materials.

2. Experimental Procedure
2.1. Materials

Graphite, copper chloride (Cu_2cl_3), sodium nitrate ($NaNO_3$), sulfuric acid (H_2SO_4), hydrochloric acid (HCl), potassium permanganate ($KMnO_4$), hydrogen peroxide (H_2O_2).

2.2. Synthesis of Graphene oxide (GO)

GO was prepared from natural graphite using a modified Hummers method [27]. In a typical experiment, graphite (1.5 g), $NaNO_3$ (1.5 g) and H_2SO_4 (70 mL) were mixed and stirred in an ice bath. Subsequently, 9 g of $KMnO_4$ was added slowly. The reaction mixture was warmed to 40∘C and stirred for 1 h. Water (100 mL) was then added and the temperature was increased to 90∘C for30 min. Finally, 300 mL of water was added slowly, followed by the slow addition of 10 mL of 30% H_2O_2. The reaction mixture was filtered and washed with 0.1 M HCl and water. The GO precipitate was dispersed in a water/methanol (1:5) mixture and purified with three repeated centrifugation steps at 3000 rpm for 30 min. The purified sample was dispersed in deionized water and centrifuged at 2500 rpm to obtain highly exfoliated GO sheets.

2.3 Synthesis of rGO/CuO

Pure copper oxide nanoparticle was synthesized by a chemical co-precipitation method [28]. Copper chloride was first dissolved in deionized water and stirred well for 45 minutes. Ammonium hydroxide solution was utilized as a precipitating agent which was included in drops and the pH of the solution was adjusted till 8. rGO composite was synthesized by modified hummers method. 0.5 gm of rGO is dissolved in 1ml of methanol and added to the above solution. The mixture was continuously stirred

for 2hrs. The precipitate was centrifuged and then washed with ethanol and water to remove the impurities present in it. The precipitate was kept under observation in the darkroom for 12 - 15 hours and dried at 100°C utilizing a hot air oven. The dried powders were collected, ground well for 5 minutes using a mortar and calcined at 300°C for 5 hours utilizing a hot air oven. Finally rGO/CuO nanopowder obtained.

3. Results and discussion
3.1 XRD Analysis

The XRD pattern of the CuO/rGO is shown in Fig. 1. All the peaks of the CuO can be assigned to monoclinic symmetry [15] of CuO (JCPDS Card no. 48-1548). No other peaks are found, indicating the high purity of the prepared CuO/rGO nanocomposites. The broad XRD peaks additionally imply that the sample is composed of CuO nanocrystallites. On the other hand, the XRD pattern of the prepared CuO/rGO nanocopmosites indicates an additional peak at 25.1° attributed to the (002) plane of the hexagonal graphite structure, suggesting that the reduced graphene oxide is incorporated into the CuO nanocomposites. The average crystallite size of the synthesized nanocomposites was 5.05 nm. The crystallite size were calculated by Scherrer's formula

$$D = \frac{K\lambda}{\beta cos\theta}$$
---------- (1)

Where λ is the wavelength of the X-Rays, β is the full width at half maximum, 2θ is the Bragg's diffraction angle.
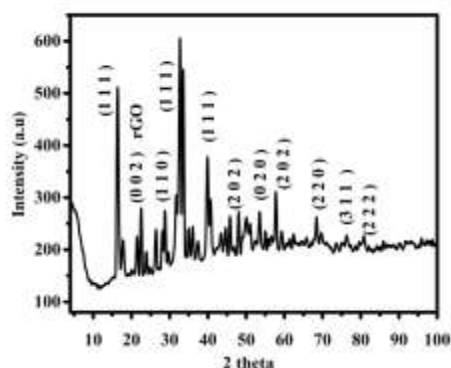

Fig. 1 XRD Pattern of rGO/CuO nanocomposites

3.2 FTIR Spectrum

The FT-IR spectra of the products are shown in Fig. 2. As indicated in Fig. 2 the wide absorption bands

between 1300 and 4000 cm^{-1} are in particular assigned to the chemisorbed and physisorbed H_2O and CO_2 molecules on the surface of the nanostructure CuO crystals. The three absorption peaks at 685, 622, 512 and 410 cm^{-1} are assigned to the Au mode and 2Bu modes, respectively. the peak at 685 and 622 cm^{-1} is possible to be from Cu–O stretching along the [101] direction [29], and the peak at 512 cm^{-1} is probably to rise up from Cu–O stretching along the [101] direction. In our previous study, throughout the calcination process, the carboxyl groups of going decompose and plenty of gases are emitted, along with CO_2, CO, and H_2O, however, there are nevertheless many –COOH [30] and –OH functional groups in graphene. For the ft-IR spectrum of CuO/rGO (Fig. 2) the stretching vibrations of C–O (1116.7 cm^{-1}), C–O (1267.45 cm^{-1}) and C=C 1615.2 and 1505.6 cm^{-1} imply that a CuO/rGO nanocomposite is obtained through chemical response.
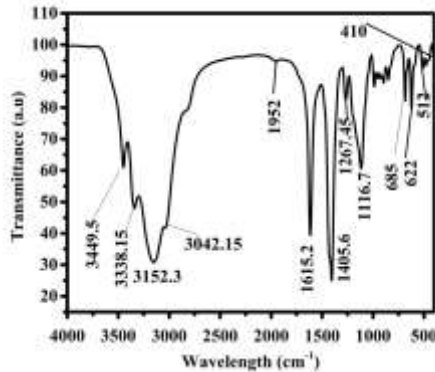

Fig. 2 FTIR Spectrum of rGO/CuO nanocomposites

3.3 UV Spectrum Analyses

The UV–vis absorption spectrum of the synthesized CuO /rGO nanocomposites is shown in Fig. 3 (a). The UV–vis absorption spectrum was recorded at room temperature for the spectral range 200–700 nm, which will carry out the absorption measurements, the samples have been dispersed in distilled water the usage of ultrasonication. The absorption spectrum reveals an absorption band at ~780 nm that is assigned to the excitonic absorption feature of CuO/rGO. the subsequent relationship between the absorption coefficient (a) and the incident photon energy (hn) absorption spectrum became used to decide the nature and value of optical band gap of CuO/rGO Nps: $(\alpha h\nu)1/n = A (h\nu-Eg)$, where A is a constant and Eg is the optical band gap of material and the value of n corresponds to $1\sqrt{2}$ and 2 for direct and indirect optical transition, respectively [31]. The direct band gap of CuO/rGO nanocomposites was calculated from $(\alpha h\nu)^2$ vs hv plot via extrapolating the straight portion of the graph on hv axis in Fig. 3b. The value of direct band gap seems to be

2.1 eV that is higher than that of the value of bulk CuO/rGO. The higher value of optical band gap of CuO/rGO nanocomposites is the direct result of quantum confinement effect at the nanoscale.
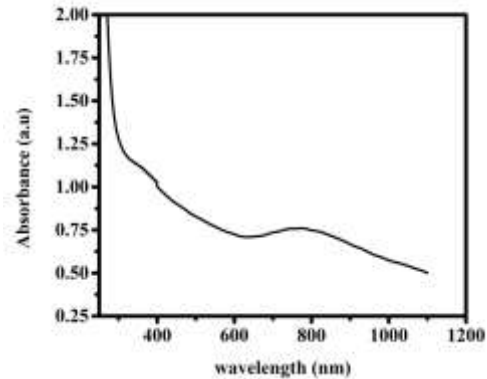

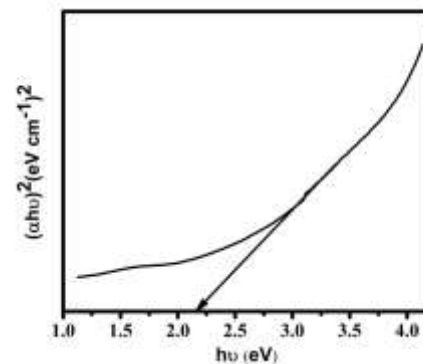**Fig. 3 (a) UV absorption spectra of rGO/CuO nanocomposites**

Fig. 3 (b) Tauc's Plot of rGO/CuO nanocomposites

3.4 SEM Analysis

The surface morphology confirms that the incorporation of Cu nanoparticle into rGO shown in Fig. 4. It is clearly inferred that the graphene particles exhibit identical ellipso- hexagon morphology. evenly distributed particles with well defined morphology could be observed. CuO nano particles are sticked on the surface of Graphene with well defined morphology. Evenly distributed particles without agglomerations were observed. Copper oxide particles with clearly agglomerated phase possessing hexagonal shapes are adsorbed on the surface of evenly distributed graphene particles.
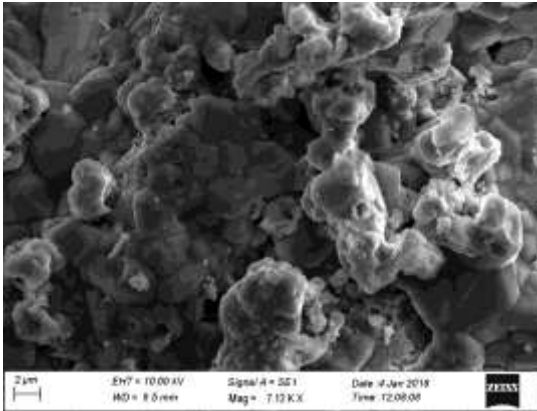
Fig. 4 SEM Image of rGO/CuO nanocomposites

3.5 Cyclic Voltametry Analysis

The performance of rGO/CuO nanocomposites was determined by cyclic voltammetry (CV), galvanostatic charge-discharge and electrochemical impedance spectroscopy (EIS). Fig. 5(a) shows the CV curves over a voltage extending from -0.5 to 0.5 V for the rGO/CuO nanoparticles measured at a scan rate of 100 mVs^{-1}. Clearly, the CV of rGO/CuO nanoparticles demonstrated a pair of Faradaic redox peaks (-0.18 V and 0.01 V). The conductive rGO/CuO encourages the charge transfer and conduction from the reactions. Conversely, the CV of RGO/CuO was a narrow rectangle, demonstrated the nonappearance of electrochemical activity and a little capacitance.
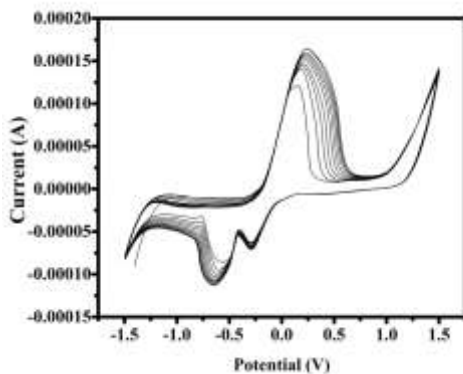

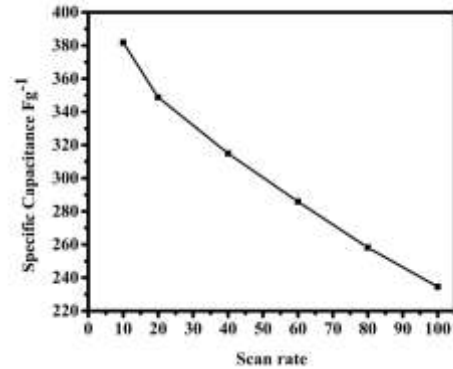Fig. 5 (a) CV Curve of rGO/CuO nanocomposites

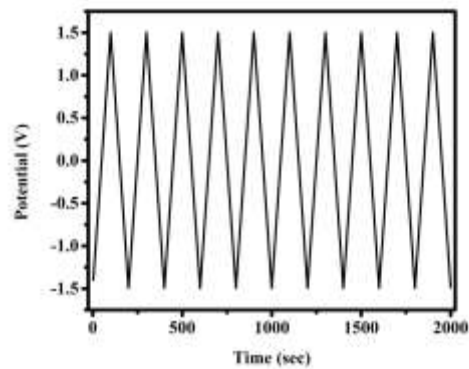Fig 5 (b) Plots of the Scan rate vs Specific capacitance of rGO/CuO nanocomposites

Fig 5 (c) Galvanostatic charge-discharge curves of rGO/CuO nanocomposites
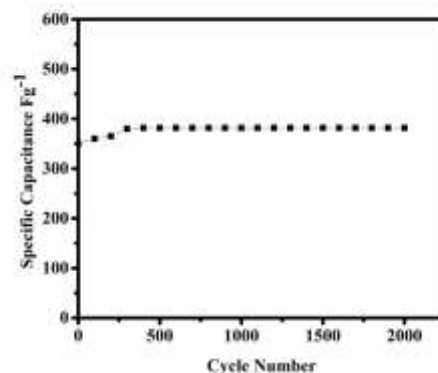

Fig 5 (d) Cycling performances of rGO/CuO nanocomposites at current density 10 Ag^{-1}
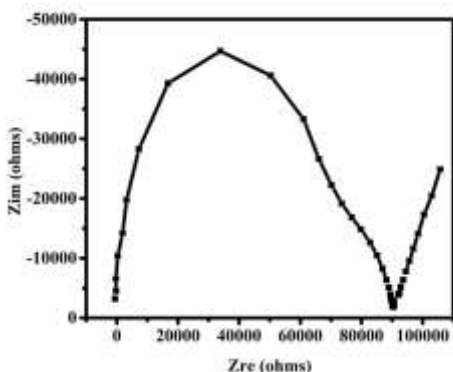
Fig. 5 (e) Nyquist Plot of rGO/CuO nanocomposites

The specific capacitance can be calculated using the following formula:

$$C = \frac{A}{M \times S_T} \qquad \text{---------------------- (2)}$$

Where C is the specific capacitance, A is the area, M is the mass of the sample, and S_r is the Scan rate.

Fig. 5 (b) demonstrates the variations in specific capacitance of the synthesized nanoparticle as a function of scan rate. The specific capacitance decreased with increasing scan rate from 10 to 100 mVs⁻¹. This is by virtue of high scan rates, diffusion limits the movement of electrolyte particles due to the time limitations, and simply the outer active surface is utilized for charge storage. At lower scan rates, despite that all the active surface area can be utilized for charge storage and the electrochemical utilization of rGO/CuO. The improvement is probably due to the unique structure of the nanoparticle. rGO/CuO gives a conductive system to electron transport amid the charge and discharge processes. rGO/CuO can enhance significantly the accessibility of the material to the electrolyte particles and abbreviate the particle diffusion and migration pathways. Along these lines, the specific capacitance of rGO/CuO nanoparticle was found to be 381.69 F/g at a scan rate of 100 mVs⁻¹ [32, 33]. Fig. 5 (c) demonstrates the charge-discharge curves of rGO/CuO nanoparticle measured at a current density of 10 Ag⁻¹. Each one of the curves was straight and symmetrical and no obvious IR drop was observed, which implies that the electrode has a less thermal resistance attributable to the very much shaped electrode/electrolyte interface. The stability and reversibility of the electrode materials are additionally in practical applications for supercapacitors. Fig. 5 (d) displays the cycling stability of rGO/CuO nanoparticle electrode inspected by the galvanostatic charge-discharge test for 2000 cycles. The outcome

exhibited the high stability and reversibility of the rGO/CuO electrode. The underlying increment of specific capacitance amid the charge-discharge cycles could be attributed to the activation process to enable the trapped cations to slowly diffuse out. Overall, the outcomes demonstrated that the rGO/CuO electrode had a substantial specific capacitance with excellent cycling stability, which is promising for the advancement of supercapacitors. Indeed, even after 2000 cycles, the capacitance observed was significantly higher than the previous reports [34-36]. EIS analysis is one of the rule strategies for analyzing the essential conduct of electrode materials for supercapacitors. The EIS data was analyzed using Nyquist plots. Every data point in the Nyquist plot has been at a different frequency. The impedance of rGO/CuO electrodes was estimated over the frequency range of 0.1 Hz to 100 kHz, at an open circuit potential with an ac perturbation of 5 mV. The identical arrangement resistance (ESR) can be acquired from the X-intercept of the Nyquist plots. In the Fig. 5 (e), the ESR of rGO/CuO nanoparticles 0.6 Ω demonstrates the execution of the electrode.

Conclusion

Co-precipitation method has been adopted for the synthesis of rGO/CuO nanoparticles. The present synthetic approach could be helpful for the synthesis of an assortment of metal oxide and mixed metal oxide nanostructures with desired shape and size. The attributed XRD peaks with sharp intensity affirm the high crystalline structure of rGO/CuO nanoparticles. SEM images suggest that the synthesized nanoparticles are well defined anisotropic structures. The functional groups present in the FTIR spectrum attributes the formation of rGO/CuO. The observed absorption band at ~780 nm proposes that the synthesized rGO/CuO NPs exhibit quantum confinement effect. The higher estimation of the direct band gap 2.1. eV of the synthesized nanoparticles than that of the estimation of bulk rGO/CuO is the immediate outcome of quantum confinement effect at the nanoscale. The phenomenal electrochemical capacitive conduct makes the synthesized rGO/CuO nanoparticles a vowing electrode material for high-performance supercapacitors.

References

1. C. G. Liu, Z. N. Yu, D. Neff, A. Zhamu and B. Z. Jang, Nano Lett., 2010, 10 4836–4868.
2. S. Chen, J. W. Zhu, X. D. Wu, Q. F. Han and X. Wang, ACS Nano, 2010, 4, 2822–2830.
3. B. Zhao, J. S. Song, P. Liu, W. W. Xu, T. Fang, Z. Jiao, H. J. Zhang and Y. Jiang, J. Mater. Chem., 2011, 21, 18792– 18798.
4. S. Hosogai and H. Tsutsumi, J. Power Sources, 2009, 194, 1213–1217.

5. Z. Chen, Y. C. Qin, D. Weng, Q. F. Xiao, Y. T. Peng, X. L. Wang, H. X. Li, F. Wei and Y. F. Lu, Adv. Funct. Mater., 2009, 19, 3420–3426.

6. H. Zhang and M. Zhang, Mater. Chem. Phys., 2008, 108, 184– 187.

7. J. Zhang, J. Liu, Q. Peng, X. Wang and Y. Li, Chem. Mater., 2006, 18, 867–871.

8. G. Derrien, J. Hassoun, S. Panero and B. Scrosati, Adv. Mater., 2007, 19, 2336–2340.

9. Y. Lu, Y. Wang, Y. Q. Zou, Z. Jiao, B. Zhao, Y. Q. He and M. H. Wu, Electrochem. Commun., 2010, 12, 101–105.

10. J. Y. Xiang, J. P. Tu, L. Zhang, Y. Zhou, X. L. Wang and S. J. Shi, Electrochim. Acta, 2010, 55, 1820–1824.

11. J. Y. Xiang, X. L. Wang, X. H. Xia, L. Zhang, Y. Zhou, S. J. Shi and J. P. Tu, Electrochim. Acta, 2010, 55, 4921–4925.

12. R. K. Bedi and I. Singh, ACS Appl. Mater. Interfaces, 2010, 2, 1361–1368.

13. L. P. Xu, S. Sithambaram, Y. S. Zhang, C. H. Chen, L. Jin, R. Joesten and S. L. Suib, Chem. Mater., 2009, 21, 1253–1259.

14. L. Q. Lu and Y. Wang, J. Mater. Chem., 2011, 21, 17916– 17921.

15. S. F. Zheng, J. S. Hu, L. S. Zhong, W. G. Song, L. J. Wan and Y. G. Guo, Chem. Mater., 2008, 20, 3617–3622.

16. J. C. Park, J. Kim, H. Kwon and H. Song, Adv. Mater., 2009, 21, 803–807.

17. H. X. Zhang and M. L. Zhang, Mater. Chem. Phys., 2008, 108, 184–187.372.

18. H. X. Zhang, J. Feng and M. L. Zhang, Mater. Res. Bull., 2008, 43, 3221–3226.

19. J. S. Shaikh, R. C. Pawar, A. V. Moholkar, J. H. Kim and P. S. Patil, Appl. Surf. Sci., 2011, 257, 4389–4397.

20. G. L. Wang, J. C. Huang, S. L. Chen, Y. Y. Gao and D. X. Cao, J. Power Sources, 2011, 196, 5756–5760.

21. J. Y. Xiang, J. P. Tu, J. Zhang, J. Zhong, D. Zhang and J. P. Cheng, Electrochem. Commun., 2010, 12, 1103–1107.

22. T. Lu, Y. P. Zhang, H. B. Li, L. K. Pan, Y. L. Li and Z. Sun, Electrochim. Acta, 2010, 55, 4170–4173.

23. W. Z. Bao, F. Miao, Z. Chen, H. Zhang, W. Y. Jang, C. Dames and C. N. Lau, Nat. Nanotechnol., 2009, 4, 562–566.

24. G. Peng, H. Song and X. H. Chen, Electrochem. Commun., 2009, 11, 1320–1324.

25. N. Li, Z. Y. Wang, K. K. Zhao, Z. J. Shi, S. K. Xu and Z. N. Gu, J. Nanosci. Nanotechnol., 2010, 9, 6690–6693.

26. M. Willander, K. Hasan, O. Nur, A. Zainelabdin, S. Zaman and G. Amin, J. Mater. Chem., 2012, 22, 2337–2350.

27. D. Y. Pan, S. Wang, B. Zhao, M. H. Wu, H. Zhang, Y. Wang and Z. Jiao, Chem. Mater., 2009, 21, 3136–3142.

28. O. Akhavan, E. Ghaderi, Flash photo stimulation of human neural stem cellson graphene/TiO_2 heterojunction for differentiation into neurons, Nanoscale 5(2013) 10316.

29. K. Kliche and Z. V. Popovic, Phys. Rev. B: Condens. Matter, 1990, 42, 10060–10066.

30. B. Zhao, P. Liu, Y. Jiang, D. Y. Pan, H. H. Tao, J. S. Song, T. Fang and W. W. Xu, J. Power Sources, 2012, 198, 423–427.

31. S. H. Tohidi., G. L. Grigoryan., A. J. Novinrooz: Inter. J. Mater. Res, Vol. 102, No. 10, (2011), p. 1247.

32. Y.P. Zhang, H.B. Li, L.K. Pan, T. Lu, Z. Sun, Capacitive behavior of grapheme ZnO composite film for supercapacitors, J. Electroanal. Chem. 634 (2009) 68.

33. Y.L. Chen, Z.A. Hu, Y.Q. Chang, H.W. Wang, Z.Y. Zhang, Y.Y. Yang, H.Y. Wu, Zinc oxide/reduced graphene oxide composites and electrochemical capacitance enhanced by homogeneous incorporation of reduced graphene oxide sheets in zinc oxide matrix, J. Phys. Chem. C 115 (2011) 2563.

34. T. Lu, Y.P. Zhang, H.B. Li, L.K. Pan, Y.L. Li, Z. Sun, Electrochemical behaviors of graphene–ZnO and graphene–SnO_2composite films for supercapacitors, Electrochim. Acta 55 (2010) 4170.

35. T. Lu, L.K. Pan, H.B. Li, G. Zhu, T. Lv, X. Liu, Z. Sun, T. Chen, D.H.C. Chua, Microwave-assisted synthesis of graphene–ZnO composite for electrochemical supercapacitors, J. Alloy Compd. 509 (2011) 5488.

36. J. Wang, Z. Gao, Z. Li, B. Wang, Y. Yan, Q. Liu, T. Mann, M. Zhang, Z. Jiang, Green synthesis of graphene nanosheets/ZnO composites and electrochemical properties, J. Solid State Chem. 184 (2011) 1421.